Journal of Mechanics Engineering and Automation 2 (2012) 411-421

Experimental and Finite Element Analysis of a T-Joint Welding

Rabih Kamal Kassab[1], Henri Champliaud[1], Ngan Van Lê[1], Jacques Lanteigne[2] and Marc Thomas[1]

1. Mechanical Engineering Department, École de Technologie Supérieure, Montreal, QC H3C 1K3, Canada

2. Institut de Recherche d'Hydro Québec, Varennes, QC J3X 1S1, Canada

Received: May 23, 2012 / Accepted: June 21, 2012 / Published: July 25, 2012.

Abstract: This paper presents the Finite Element (FE) modeling of a two-seam welding process for a T-joint with a V chamfer preparation. The aim of the model is to predict the deformations, distortions and residual stresses resulting from the welding of the plates and experiments have been carried out in order to compare to the FE model. The "birth and death" method is used in ANSYS© to simulate the filler metal deposition and the heat generation and weld pool simulation are conducted accordingly with the double ellipsoid configuration as proposed by Goldak et al. The model takes into consideration the temperature dependent non-linear material properties and uses a new formulation to compute the temperature dependent combined coefficient of heat loss. Improvements in the calculation are achieved by combining two types of meshing. The FE simulation is divided into two consecutive parts: the thermal simulation followed by the structural simulation. The results of the numerical model are compared to experiments.

Key words: Welding, T-joint, finite element modeling, residual stresses.

1. Introduction

Anticipating the residual stresses and the distortions is very important for the welded structures and this study is a part of a larger project that deals with welding simulation, residual stress and distortion computations in the welded joints and structures. Beyond a better understanding of the distortion in a T-joint assembly, this study is aimed at improving hydraulic Francis turbines manufacturing. Assembling Francis turbine runner by welding can result in a distorted runner that requires post-welding heat treatment to reduce the distortions and to minimize subsequent machining. The authors' goal is to build a reliable finite element model of a T-joint welding assembly in order to predict the residual stresses and the distortions due to the metal deposition process. The FE model will be compared and validated with an experimental two-sided weld T-joint.

In FE welding simulations, the first 2D model of a heat source appeared 25 years ago. Quite recently, with increased hardware computation capabilities, more efficient algorithms and 3D models begin to appear. Muraki (1975) developed the first finite element codes for welding simulation [1]. In 1990, Karlsson and Josefson made a single pass butt welding simulation [1] and in 1996, Murthy et al. proposed a detailed methodology for the analysis of residual stresses due to welding and quenching processes [1]. In 1996, Mackerle made an exhaustive bibliography about finite element analysis and simulation of welding from 1976 till 1996 [2]. Later in 1999, the metallurgical transformations were taken into consideration by Framatome and EDF [1].

Additionally, the heat source models were improved through subsequent researches. First there were the uni-dimensional models such as point and line heat sources and two-dimensional models such as plane

Rabih Kamal Kassab, master student, research field: structural finite element analysis.

Corresponding author: Henri Champliaud, professor, Ph.D., research fields: finite element modeling and simulation. E-mail: henri.champliaud@etsmtl.ca.

heat source that considered the heat intensity and temperature infinite at the source. These models gave acceptable results only in the regions where the temperature is 20% less than the melting temperature. A new model was proposed by Pavelic (1965) who suggested a Gaussian heat distribution on a circular disc [3]. This model gave a more realistic model with better heat distribution in the Melted Zone (MZ), and it was very accurate in the case of a torch that did not cause any melting of the metal (Fig. 1).

The heat distribution in Pavelic disc is given by

$$q_{(r)} = q_{(0)} e^{-cr^2} \quad (1)$$

where:

- $q(r)$ = surface flux at radius r (W/m^2);
- $q(0)$ = maximal flux at source center (W/m^2);
- r = radial distance from center (m);
- c = concentration coefficient (m^{-2}).

For the same input energy, the higher is c, the smaller is the hot spot diameter of the arc flame (Fig. 1).

This disc is later expressed in a local coordinate system (x, ξ) instead of (x, z) moving with the torch where $\xi = z + v*(\tau - t)$ where ξ and z are vectors in heat source direction, t is time and is τ a lag factor needed to define the position of the source at time $t = 0$.

The simplest 3D model of a heat source is the half spherical model. It is expressed with

$$q(x, y, \xi) = \frac{6\sqrt{3}Q}{\pi c^3 \sqrt{\pi}} e^{\frac{-3x^2}{c^2}} e^{\frac{-3y^2}{c^2}} e^{\frac{-3\xi^2}{c^2}} \quad (2)$$

where $Q = \eta \cdot V \cdot I$ is the total amount of energy put inside the half sphere, η is the efficiency of the process, V is the voltage (Volt) and I the current (A) of the heat source. This model is a particular case of an ellipsoid heat source that can be expressed by

$$q(x, y, z, t) = \frac{6\sqrt{3}Q}{abc\pi\sqrt{\pi}} e^{-\frac{3x^2}{a^2}} e^{-\frac{3y^2}{b^2}} e^{-\frac{3(z+v(\tau-t))^2}{c^2}} \quad (3)$$

An even more general model can be expressed by the double ellipsoid [3-4]. It is able to give better results for the temperature distribution in the melted zone. The double ellipsoid model is made of two ellipsoidal quarters: One is in the upstream while the other is in the downstream of the weld pool centre in the direction of the weld progression (Fig. 2).

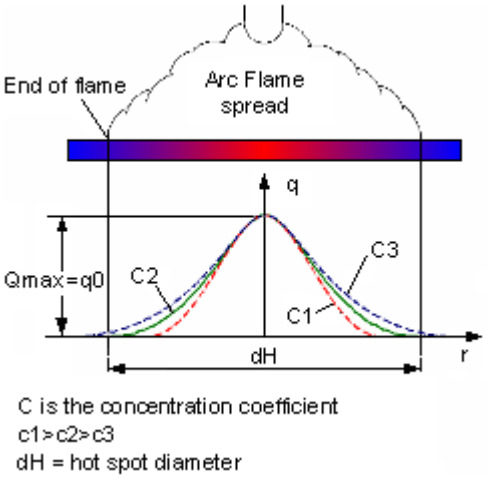

Fig. 1 Pavelic disc [3].

The heat distribution is divided unequally between the two quarters using two parameters f_f and f_r where f_f and f_r are the proportions of heat in the frontal (upstream) quarter and in the rear (downstream) quarter respectively with $f_f + f_r = 2$.

These two parameters are determined experimentally [3-4].

The heat equations are

$$q_f(x, y, z, t) = \frac{6\sqrt{3}f_f Q}{abc\pi\sqrt{\pi}} e^{-\frac{3x^2}{a^2}} e^{-\frac{3y^2}{b^2}} e^{-\frac{3(z+v(\tau-t))^2}{c^2}} \quad (4)$$

$$q_r(x, y, z, t) = \frac{6\sqrt{3}f_r Q}{abc\pi\sqrt{\pi}} e^{-\frac{3x^2}{a^2}} e^{-\frac{3y^2}{b^2}} e^{-\frac{3(z+v(\tau-t))^2}{c^2}} \quad (5)$$

In this paper, the above double ellipsoid configuration is used for heat generation in the weld pool and the "birth and death" method is implemented to simulate filling metal deposition.

First a description of the experimental test will be briefly presented with the related results that will be useful for comparison; then the FE model will be described with its approximations and results. Furthermore, a new formula is suggested for the calculation of the combined heat loss coefficient. Then, a comparison between the FE model and the experimental tests will show the strength and the weakness of the simulations. Finally, suggestions of possible improvements for future works are presented.

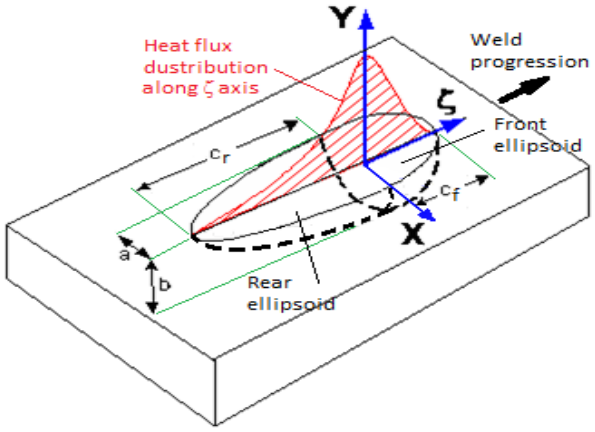

Fig. 2 Double ellipsoid heat input source [3].

2. Experimental Tests

The T-joint is made of AISI-1018 steel plates of 3/8 of inch (9.5 mm) in thickness and 10 inches in length (254 mm). The width is 10 inches (254 mm) for the Horizontal Plate (HP) and 6 inches (152.4 mm) for the Vertical Plate (VP). The 6 inch wide plate is symmetrically V chamfered at one end with a ¼ inch (6.35 mm) height X 30 degree angle and is welded perpendicularly and along the center of the other plate (Fig. 3).

A SCOMPI™ robot is used for the welding process and the plates are placed in a special fixture allowing the robot to make a flat single weld pass on each side with cooling time in between. The parameters of the welding are 26.9 Volts and 220 Amps with a torch speed of 5 mm/s. The welding efficiency is estimated at $\eta = 77\%$.

Thermal records and structural measurements were done. For thermal records, a real time temperature acquisition was made during the welding process. For structural measurements, strain deformations of a rosette (hole-drilling technique) were taken in order to compute the residual stresses at one point in the structure. The final distortion of the assembly was also measured.

2.1 Temperature Acquisition

The acquisition is made using 8 thermocouples, 4 on each plate (Fig. 4).

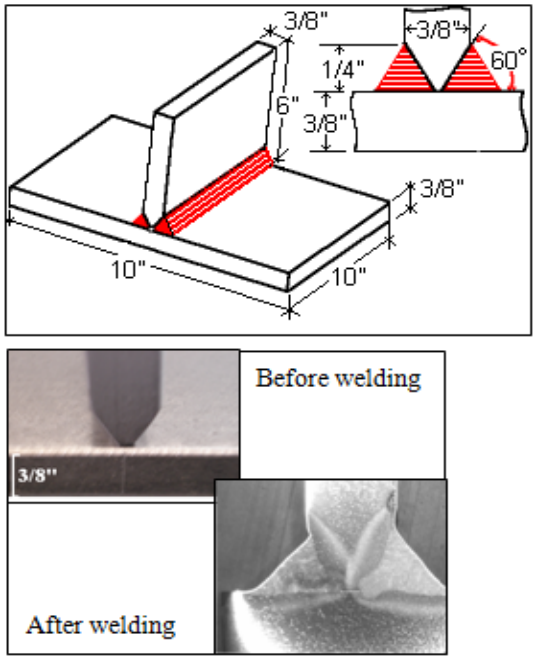

Fig. 3 Joint geometry.

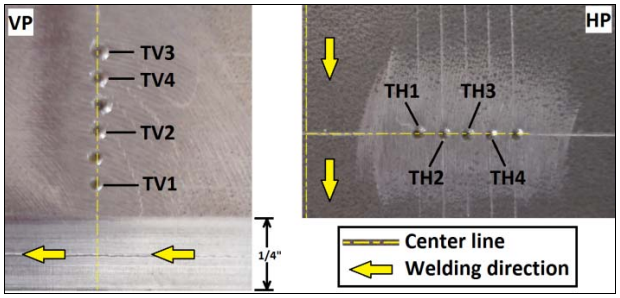

Fig. 4 Thermocouples locations on VP and HP (the center lines on both plates can be seen).

The thermocouples positions are located on the plate's faces and they are noted TV1 to TV4 from the nearest thermocouple to the farthest from the weld seam on the VP. A similar arrangement is used for TH1 to TH4 on the HP. All the thermocouples are located halfway of the T-joint length.

Only the temperature readings during the second pass are used for comparison because of the excessive direct radiation of the heat source on the thermocouples that occurs during the first pass where the thermocouples and the torch are on the same side about the VP. Furthermore, the readings at TV1 are discarded because of the failure of the bonding cement at this location. Fig. 5 shows the variation of the temperature recorded during the first and the second welding pass.

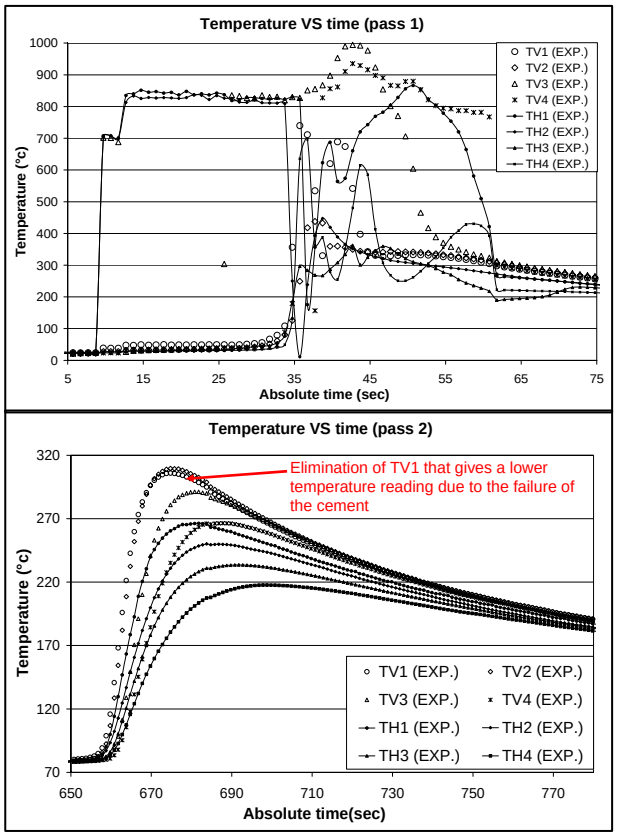

Fig. 5 Temperature acquisition.

2.2 Structural Measurements and Results

The structural measurements consist of calculating the residual stress at the center point on the HP surface opposite to the welded VP (Fig. 6) and of measuring the distortion of the HP.

The residual stress calculation is done using the hole-drilling strain gage method. Briefly, this technique consists of measuring the deformations around a hole drilled at the center of a strain gage rosette (Fig. 6).

Drilling a hole in a stressed steel results in deformations around and near the hole caused by the stress relief in this area. More information about this technique can be found in Ref. [5] and ASTM E837-92. The following are the main results, where β is the angle between $S1$ and x direction: $\sigma_{max} \equiv S1 = 429$ MPa and $\sigma_{min} \equiv S3 = 60$ MPa and $\beta = 13°$.

The expected error on this measurement can vary between 10% and 30% when the residual stress exceeds 70% of the material elastic limit [5] which is

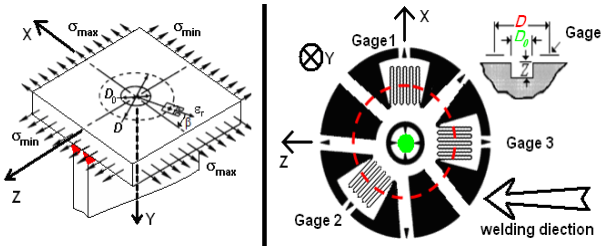

Fig. 6 Global and directional position of the strain gage rosette.

the case at the measured point (due to permanent deformation of HP).

The distortion measurement is a direct measure of the displacements of the HP sides in the y direction (Fig. 7).

The following measures are obtained by keeping the VP vertical. The displacement on the side of the first pass is +1.35 mm and the one on the side of the second pass is +3.13 mm. Note that the heat effect of the second pass produces stress relief in the first cordon.

3. Finite Element Model Description

The finite element model is based on three main assumptions. The first assumption is related to the thermal and structural boundary conditions introduced by the fixture of the joint: The flexibility of the joint and its heating up during the welding are not taken into account by the model. The second approximation is related to the values of the temperature dependent thermo-physical properties of the material: These values are determined experimentally and they vary from one reference to another [6-12]. The welding procedure efficiency is the third important assumption: There is no experimental direct method used to calculate the welding efficiency to be applied in the simulation; thus an approximated value is first used and then adjusted after several iterations according to the temperature matching with the thermocouples.

Table 1 presents the parameters values used in the FE model for the welding process and for the double ellipsoid heat source.

Fig. 8 shows the graphical thermo-physical properties of the AISI-1018 used in the simulation. Most of these values are found in Refs. [6-12] for a low carbon steel.

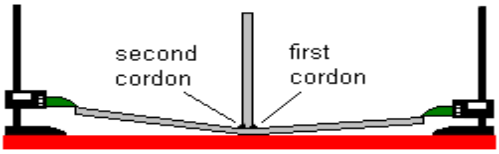

Fig. 7 Distortion measurement.

Table 1 Welding process and double ellipsoid parameters.

Welding parameter	Value	Double ellipsoid parameter	Value
v (mm/sec)	5	a (mm)	3.666
I (A)	220	b (mm)	6.350
V (V)	26.9	$c1$ (mm)	$2a$
η (%)	77.0	$c2$ (mm)	$4a$
		f_f	0.6
		f_r	1.4

The Double Ellipsoid (DE) dimensions are determined experimentally by measuring the size of the weld pool using the microscopic photography of the joint section showing the borders of the weld pool and of the HAZ (Heat Affected Zone) (Fig. 3).

For the thermal conduction coefficient, the only reference found for AISI-1018 at liquidus temperature is Ref. [10] where it is mentioned that k = 31.2 W/m°C. Ref. [9] mentions 259.3 W/m°C for a low carbon steel in the same condition. In fact, this big difference is due to a fictive added value to simulate convection and turbulence in the weld pool.

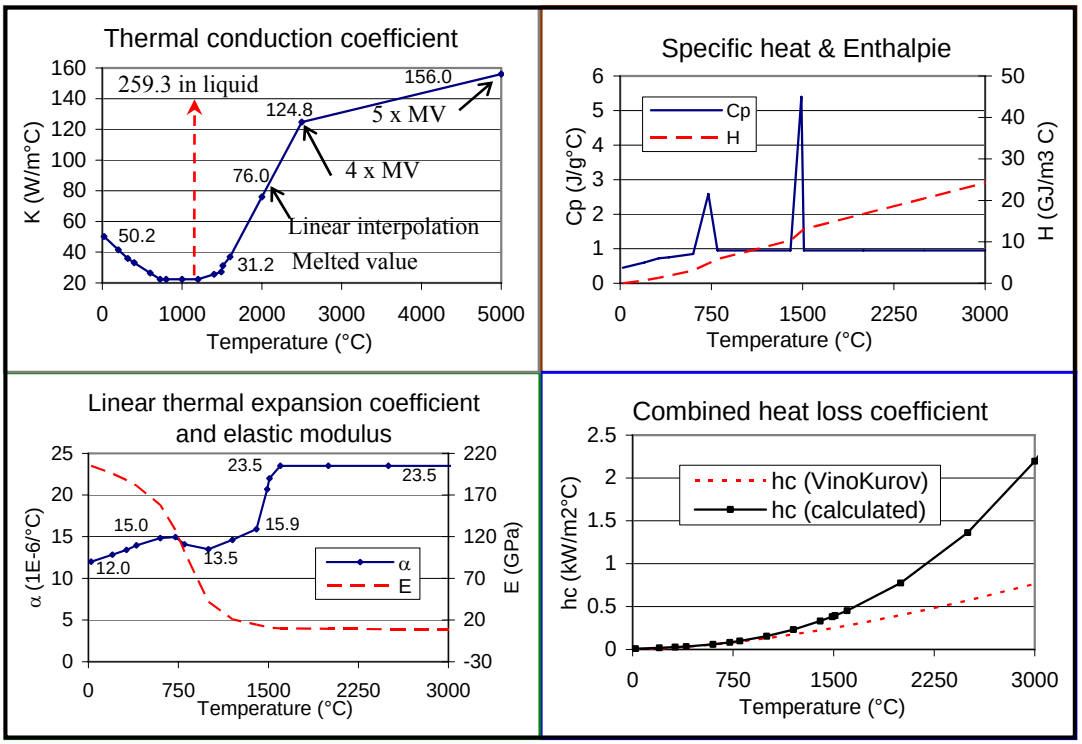

Fig. 8 Thermo-physical properties of the AISI steel used in the simulation.

ANSYS uses the enthalpy, and not the specific heat to calculate the temperatures. The enthalpy H is numerically calculated using

$$H = \int_{T1}^{T2} \rho C_p \, \mathrm{dT} \qquad (6)$$

where $T1$ and $T2$ are the temperatures between which the variation of H, $\Delta H = HT2 - HT1$, is calculated, ρ is the density and C_p is the temperature dependent function of the specific heat.

As it is mentioned previously, several iterations are necessary to obtain the values that give a better fit between the simulated temperatures and the measured ones. Temperature controlled tensile tests are performed to determine the elastic modulus and the Elastic Limit (EL) of AISI-1018 at 5 different temperatures: (T; EL) = ([20, 203, 420, 608, 802]; [474, 464, 389, 189, 41.5]).

The combined heat loss factor is calculated using the following formula:

$$h_c = h_f + \varepsilon\sigma(T^2 + T_f^2)(T + T_f) \qquad (7)$$

where T is in Kelvin, h_f is the convection coefficient, ε is the emissivity and σ is the Stefan-Boltzmann constant which equals 5.67×10^{-8} J m^{-2}s^{-1}K^{-4}.

By comparing the results given by this formula with others given by another formula as suggested by Vinokurov [4], $h_c = 24.1\times10^{-4}\times\varepsilon\times T^{1.61}$, it is found that the results obtained using Eq. (7) are more accurate, thus Eq. (7) is used to evaluate the temperature dependent h_c during the welding process simulation.

The meshing of the geometry is shown in Fig. 9.

The geometry is divided in two regions: region 1 (the region near the HAZ (Fig. 9c) and region 2 (the regions far from the HAZ). The meshing is done by using 8-node brick elements (1 DOF, T, for the thermal element, and 3 DOF, Ux, Uy, Uz, for the corresponding structural one).

The mesh grid is fine and uniform in the nearest regions of the weld seam where occur high temperature and stress gradients and it is coarser in the farthest regions, increasing the element size in the vertical direction for the VP and in the horizontal direction for the HP (Figs. 9a-9b)). The combination of two ways of meshing (per sections and per controlled meshing size, as shown in Figs. 9a-9b)) uses the advantage of both meshing techniques by minimizing the total number of elements (per section meshing) and by helping to obtain smoother continuous results profiles through the sections (increasing meshing) without adding additional elements. Fig. 9c shows the meshing in the section near the HAZ and the meshing of the filling metal. Figs. 9d-9e show a central section of the joint and Fig. 9d shows the nodes (red dots) where the thermocouples are located in the experiment. The location of the center of the strain gage rosette is shown by a red dot on the meshing in Fig. 9e. The "birth and death" method used to simulate the deposition of the filler metal, consists of "deactivating" the elements representing the undeposited filler metal at the beginning by multiplying their rigidity matrix by 10^{-6} and later by "reactivating" them along with the torch displacement.

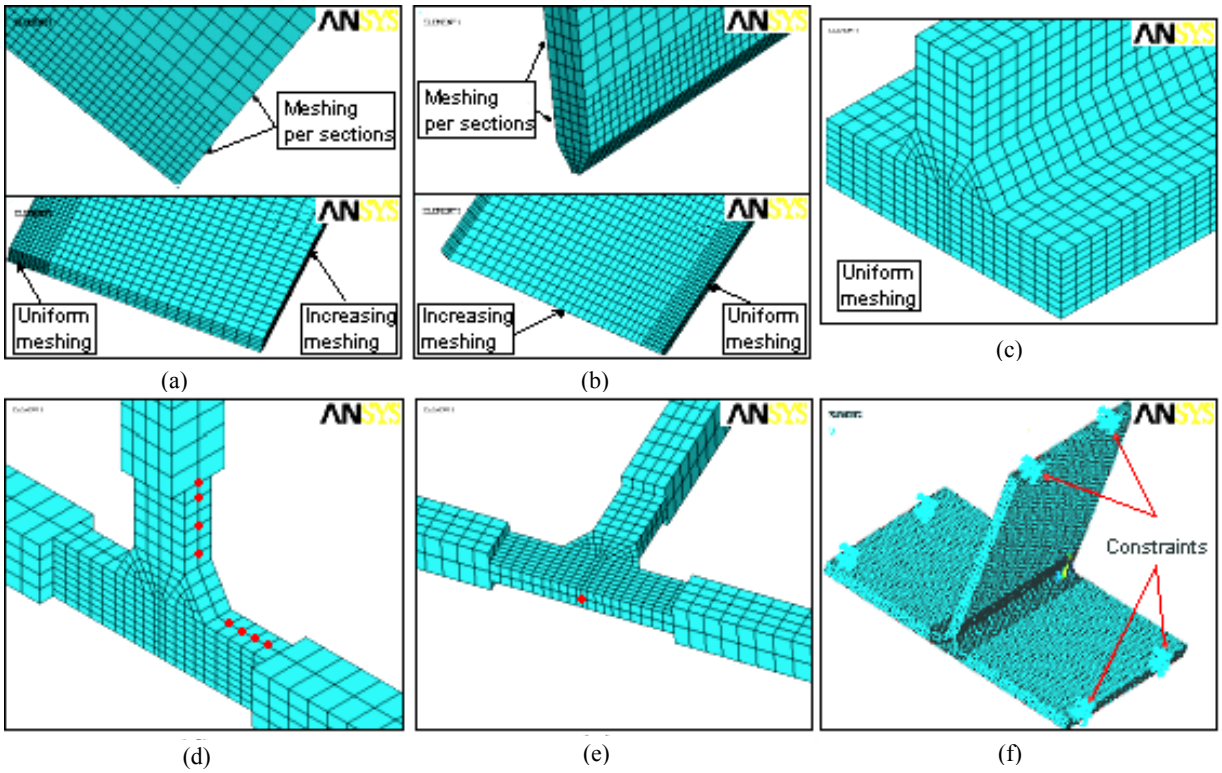

Fig. 9 Meshing: (a) HP mesh; (b) VP mesh; (c) filling metal and region 1; (d) thermocouples nodes; (e) residual stress node; (f) structural B.C.

4. Numerical Simulation Results

4.1 Thermal Simulation Results

The thermal simulation consists first of applying the thermal Boundary Conditions (B.C.) on the finite element mesh. Then, at each computed step, the elements of the weld pool are activated according to the DE location with exponential body heat in the weld pool elements.

During deposition of filler metal simulation, a higher ambient temperature T_f is considered to simulate higher air temperature around the joint when the joint is maintained inside the fixture (as mentioned at the beginning of the previous section).

Fig. 10 shows the temperatures at the nodes which match exactly the thermocouples locations on the VP and on the HP.

For comparison between the first and second pass, it is found that the thermal gradients at the nodes representing the temperature acquisition locations are higher during the first pass than the second pass in both plates. This is due to the closer distance between these locations and the first pass (comparison between Fig. 10a and Fig. 10c vs. Fig. 10b and Fig. 10d). For comparison between the VP and the HP for the second pass, the maximum reached temperatures and the temperature gradients are higher in the VP. The reason is that the thermocouples locations in the VP are closer than the one in the HP during the second pass. Furthermore, the heat flux in the HP is split between the two sides of the joint which reduces the thermal gradients in the HP. Due to the direct radiations effect on the thermocouples during the first pass, the comparison with the experimental assembly will be limited to the second pass only and for all the thermocouples nodes except for TV1 for the reason mentioned in section 2.1.

4.2 Structural Simulation Results

The first thing is the application of the structural B.C. (Fig. 9f) where the shown constraints are clamped surfaces

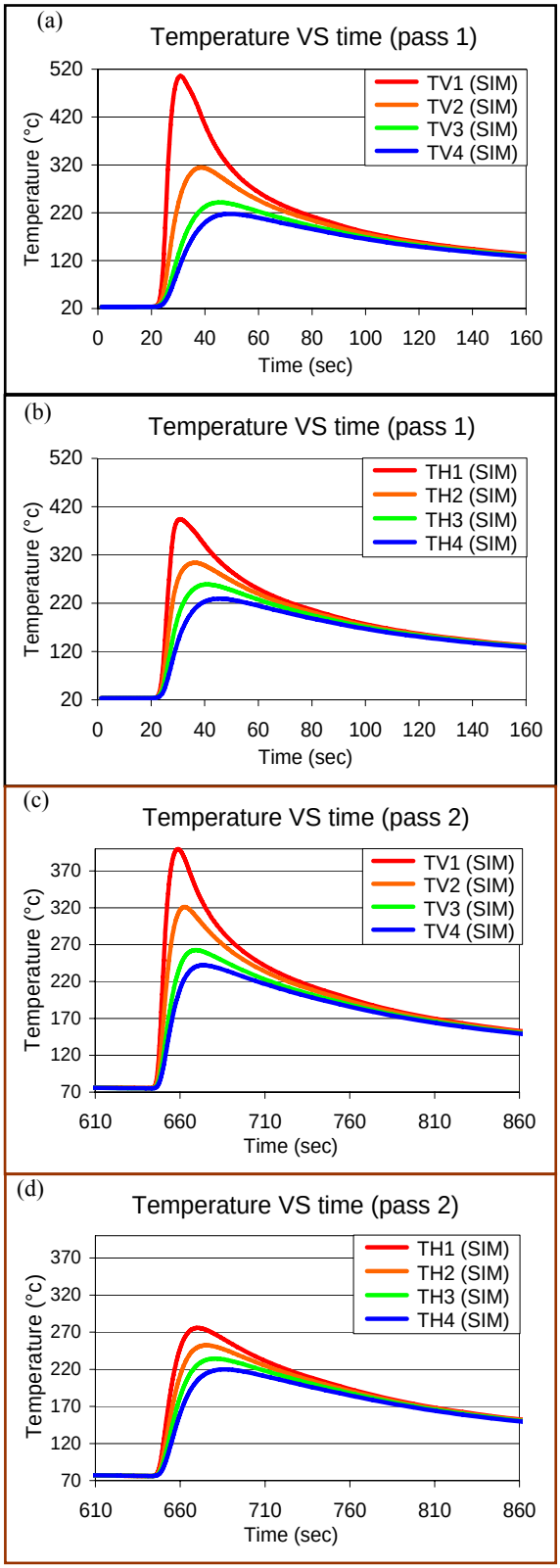

Fig. 10 Temperatures at the nodes representing the thermocouples locations: (a) pass 1 on VP; (b) pass 1 on HP; (c) pass 2 on VP; (d) pass 2 on HP.

simulating the tightened bolts. Fig. 11 shows the structural B.C. evolution during the multi-pass welding procedure.

The nodal temperatures obtained from the thermal simulation are applied to the nodes in the structural simulation as thermal loads for each step. At the final step, all the temperatures are set to the initial temperature T_f, i.e., the all assembly is brought back to the ambient temperature.

Table 2 shows the residual stress state at the specified point shown in Fig. 9e. Comparing the out-of-plane component $Sy = 75.7$ MPa to the theoretical value of zero gives the FE accuracy of 75.7/457 = 16.6% with respect to maximum stress of 457 MPa. This is due to the fact that element size is not fine enough (a finer mesh will require longer computation time).

It is found that the stresses *Sx*, *Sy* and *Sz* coincide almost exactly with the principal stresses *S*1, *S*3 and *S*2 respectively.

About the displacements of the HP sides they are 0.93 mm for the displacement on the side of the first pass, and 2.1 mm on the side of the second pass.

5. Comparison between the Simulation and the Experiments

5.1 Comparison of the Thermal Results

Fig. 12 shows the comparison between the simulated temperatures (SIM) and the experimentally recorded (EXP.) on the VP.

The results do not match exactly and have different gradients. The temperature gradients in the simulation are higher than the ones in the experiment: The two lower simulated temperature values, TV3 (SIM) and TV4 (SIM), are lower than their respective experimental values while TV2 (SIM) is higher than TV2 (EXP).

Furthermore, same experimental temperature gradient rate will lead to TV1 (SIM) higher than TV1 (EXP).

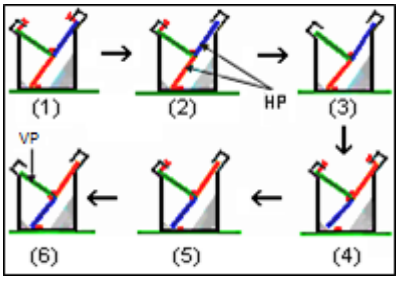

Fig. 11 Evolution of structural B.C.

Table 2 Residual stress state.

Measured residual stresses (MPa)						
Sx	*Sy*	*Sz*	*S*1	*S*2	*S*3	Von-Mises
457	75.7	409	458	409	75.6	360

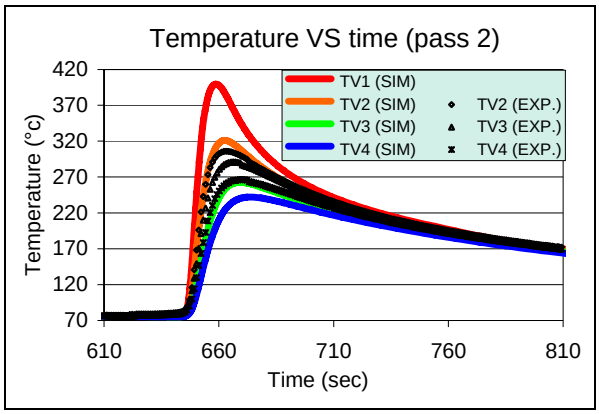

Fig. 12 Comparison of TV.

The reason for this gradients' difference could be explained by the presence of the important amount of heat flux transferred to the plates without passing through the weld pool. This has a significant effect especially in a T-joint like configuration (Fig. 13).

It can be seen that the effect of the radiation is more important in Fig. 13b than Fig. 13a, which affects significantly the absorbed heat distribution. This amount of radiation cannot be neglected or excluded and, thus, it is added in the weld pool in the double ellipsoid simulation. This results in increasing the gradients near the weld cordon. During the second pass, the readings of the thermocouples on the VP are affected by the indirect presence of the radiation (radiation then conduction through the thickness of the VP). For the TV (EXP), the difference between TV3 and TV4 is 25 °C while the distance between the thermocouples TV3 and TV4 is 2.73 mm. In the other

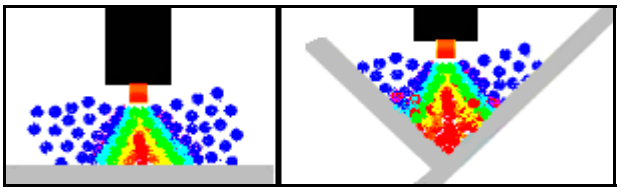

Fig. 13 Radiation in a corner VS in a flat wall.

hand, the difference between TV2 and TV3 is 15°C while the distance between the thermocouples TV2 and TV3 is 4.45 mm. Thus we are stepping toward the direction of the lower gradients but we are obtaining higher gradients. The effect of the radiation is not clearly understood in the regions very close to the weld pool.

This effect does not exist for the thermocouples on the HP during the second pass. Fig. 14 shows a quasi-perfect matching between the temperatures TH (SIM) and TH (EXP).

The maximum difference is for the peak of TH1 and it is only of 9 °C. This difference shows up and disappears in a short period of 30 seconds.

5.2 Comparison of the Structural Results

Table 3 contains the structural results comparison for the residual stress state at one specified point and for the displacements at the lateral tips of the HP.

The difference on the first principal stress *S*1 is +29 MPa which is in excellent agreement and both results are close to yield stress (475 MPa). On the other hand, a big gap of +349 MPa is found for the longitudinal direction. The error is mainly due to the measurement technique, for it is well known that when the residual stress exceeds 70% on the elastic limit of the material, an error of up to 30% is expected for the hole-drilling technique.

Concerning the differences on the displacements, they are related to the fixture elasticity in the experiment versus the infinitely rigid fixture (zero displacements) applied as structural boundary conditions in the simulation. Modeling the fixture stiffness will introduces new assumptions and / or makes the FE model more complicated with inefficient

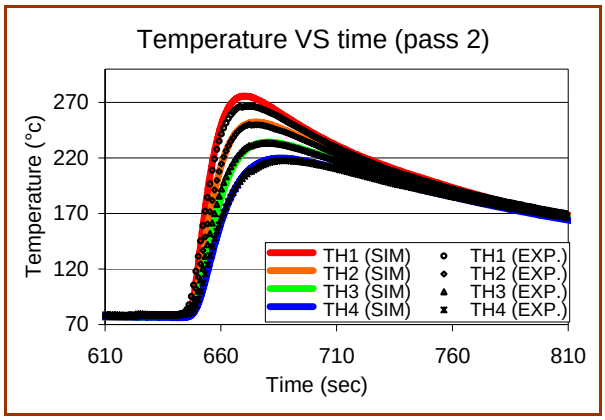

Fig. 14 Comparison of TH.

Table 3 Structural results comparison.

	SIM	EXP	Error
Stress (MPa)			
Sx	458	429	+29
Sy	409	60	+349
Displacements (mm)			
Pass 1 side	0.93	1.35	31.1%
Pass 2 side	2.1	3.13	32.9%

simulation time. The displacements were proportional at both sides with higher displacements for the experimental model.

5.3 Graphical Results of the FE Model

An important advantage of FE modeling is to be able to re-do the simulation with different parameters, re-run the analysis, and obtain global plots for any region at any time and not only at specific points. The results can be presented easily as readable plots and graphics of the studied structure.

Fig. 15 shows the displacements of the sides of the HP during all the welding simulation until 1440 seconds where the maximum temperature in the structure is 85 °C and the values of the material properties are very close to their values at the ambient temperature. It shows the releasing and the clamping times of the plates are clearly noticeable with the instantaneous displacements. These displacements of the HP sides are symmetrical about the joint during the variation of the structural B.C. and till the beginning of the final cooling. It also shows the effect of cooling that produces an asymptotical shape in the displacements

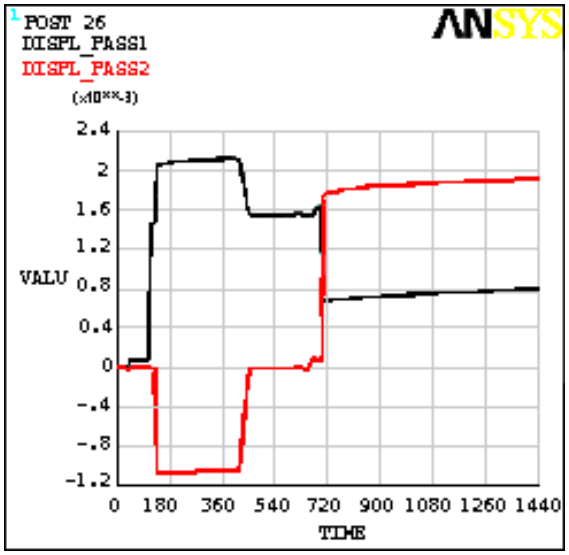

Fig. 15 Displacements of the sides of the HP in *y* direction.

curves towards a steady value of the residual deformed and distorted shape.

Fig. 16a presents the last step in the thermal simulation and Fig. 16b presents the Von-Mises residual stress state in the 50 mm neighboring region around the weld. Also, a central cross section of the joint demonstrates the relieved stresses in the first pass in comparison with the second pass Fig. 16c.

6. Conclusions and Recommendations

In this study, the modeling of a T-joint welding presenting a V preparation was done. The simulated model was done using ANSYS© software with the "birth and death" method to simulate the filler metal deposition, also it uses the double ellipsoid model to simulate the heat in the weld pool.

For the simulation, the temperature dependent thermo-physical material properties are taken in consideration. A new formula has been presented for the evaluation of the combined heat loss coefficient.

Then the FE model is compared with an experimental test in the welding laboratory. Both models contain two parts: thermal part and structural part. The result summary is as follows:

- Higher gradients on the VP temperatures given by the FE model are observed due to the radiation effects that the heat source model does not include. In the other hand, it was obtained a nearly perfect match for the temperatures of the HP where the radiation does not have a significant effect;
- The FE model compares very well the residual stress state at a specified point with an error of only +29 MPa on the first principal stress and +15.6 MPa on the

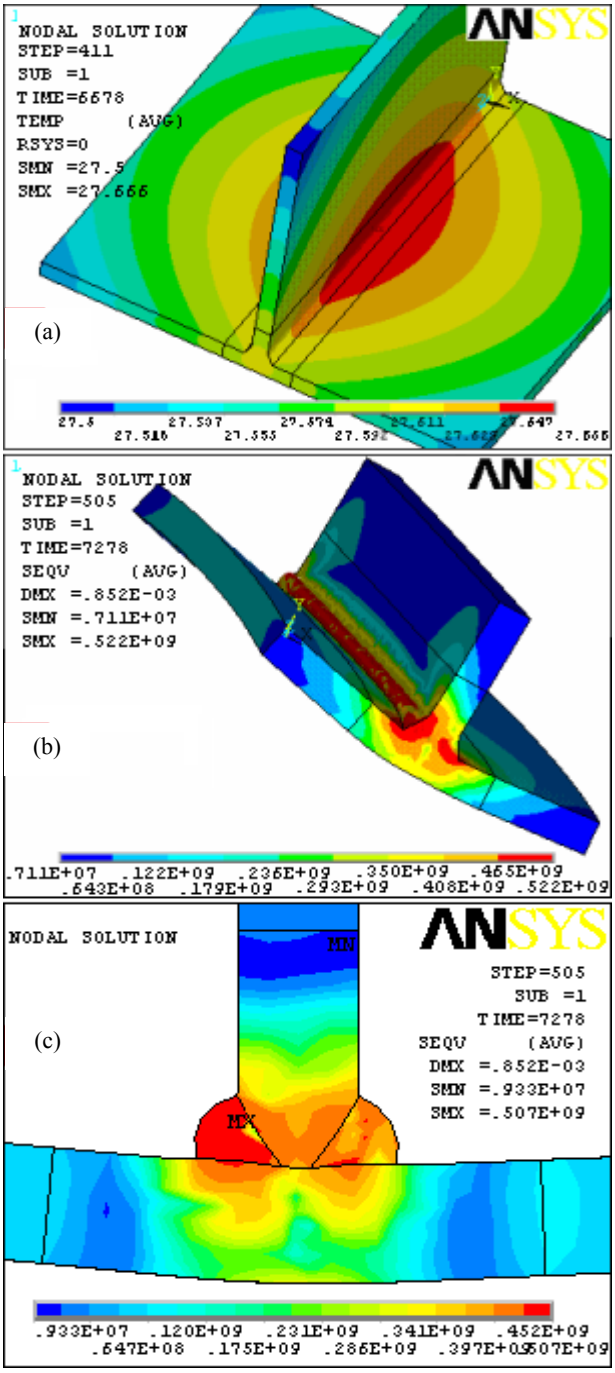

Fig. 16 Last step in the thermal simulation (a) and residual Von-Mises stress in 50 mm regions around the joint (b) and (c).

third principal stress (this means no more than at 6% deviation in comparison with the elastic limit at room temperature). About the displacements measures, errors of 31.1% and 32.9% are observed on the first pass side and on the second pass side respectively. This is due to the elastic fixture used in the experiment that is modeled as infinitely rigid with zero displacements constraints in the FE model.

The ease to vary the geometrical, thermal and structural parameters makes it flexible to represent the welding of several similar joints. This model can be used to improve the welding process by varying its parameters; such as the preparation's geometry, the current and voltage, the simultaneous deposit of several beads, the torch's speed, etc.

Modeling more complex heat sources with parametric geometrical shapes can be developed to fit more with specific welding pools profiles with irregular penetration shapes. This could be a possible improvement useful in modeling the nail shape observed during the second pass like shown in Fig. 3. In the same way, the introduction of the radiation effect in the cases where the radiation cannot be neglected will help in having more accurate results near the weld pool Improvements on the data acquisition like using thermography for temperature acquisition can help a lot in having more accurate and dependable verification data.

More advanced experiments are needed to have more reliable comparison data. Working on more complex types of heat sources such as irregular shapes and radiation effect will be necessary for the subsequent works to take welding simulation at a higher level.

Acknowledgments

The authors wish to acknowledge the NSERC for the funding. They also wish to thank the Institute of Research of Electricity of Quebec (IREQ) for the tests done to determine the yield limit of the material at different temperatures used for the welded joint experiment.

References

[1] A. Yaghi, A. Becker, State of the art review—weld simulation using finite element methods, Project FENET EU Thematic Network, School of Mechanical, Materials & Manufacturing Engineering, University of Nottingham, UK, 2004.

[2] J. Mackerle, Finite element analysis and simulation of welding: A bibliography (1976-1996), Modelling Simul. Mater. Sci. Eng. 4 (1996) 501-533.

[3] J. Goldak, A. Chakravarti, M. Bibby, A new finite element model for welding heat sources, Metallurgical and Materials Transactions B 15 (1984) 299-305.

[4] J. Goldak, M. Bibby, J. Moore, R. House, B. Patel, Computer Modeling of Heat Flow in Welds, Metallurgical Transactions B 17 (1986) 587-600.

[5] Measurements Group, Measurements Group Tech Note TN-503, Measurement of Residual Stresses by the Hole-Drilling Strain Gage Method.

[6] A. Goldsmith, T.E. Waterman, H.J. Hirschhorn, Handbook of Thermophysical Properties of Solid Materials, The Macmillan Company, New York, Vol. 3, 1961.

[7] R. Becker, Structural behavior of simple steel structures with non-uniform longitudinal temperature distributions under fire conditions, Fire Safety Journal 37 (2002) 495-515.

[8] S.-H. Cho, J.-W. Kim, Analysis of residual rtress in carbon steel weldment incorporating phase transformations, Science and Technolody of Welding and Joining 7 (2002) 212-216.

[9] S. Koric, B.G. Thomas, Efficient thermo-mechanical model for solidification processes, International Journal for Numerical Methods in Engineering 66 (2006) 1955-1989.

[10] S. Ahn, Modeling, Estimation, and control of electroslag remelting process, Master's Thesis, The University of Texas at Austin, 2005.

[11] Y.S. Touloukian, Thermophysical Properties of Matter: The TPRC Data Series, Vol. 1, 4 & 12.

[12] Y.S. Touloukian, Thermophysical Properties of High Temperature Solid Materials, Vol. 3: Ferrous Alloys, 1966.